

Orbital-selective correlation effects and superconducting pairing symmetry in a multiorbital t - J model for bilayer nickelates

Guijing Duan,¹ Zhiguang Liao,¹ Lei Chen,^{2,3} Yiming Wang,² Rong Yu,^{1,4,*} and Qimiao Si^{2,†}

¹*Department of Physics and Beijing Key Laboratory of Opto-electronic Functional Materials & Micro-nano Devices, Renmin University of China, Beijing 100872, China*

²*Department of Physics & Astronomy, Extreme Quantum Materials Alliance, Smalley Curl Institute, Rice University, Houston, Texas 77005, USA*

³*Department of Physics and Astronomy, Stony Brook University, Stony Brook, NY 11794, USA*

⁴*Key Laboratory of Quantum State Construction and Manipulation (Ministry of Education), Renmin University of China, Beijing, 100872, China*

The recent discovery of superconductivity in $\text{La}_3\text{Ni}_2\text{O}_7$ raises key questions about its mechanism and the nature of pairing symmetry. This system is believed to be described by a bilayer two-orbital Hubbard model. The considerations of orbital-selective Mott correlations motivate a bilayer two-orbital t - J model and, accordingly, we study the superconducting pairing in this model. We obtain an overall phase diagram of superconductivity, where the leading channel has either extended s -wave or $d_{x^2-y^2}$ -wave symmetry. Our analysis highlights how the orbital-selective correlations affect the superconducting pairing via the interlayer exchange couplings and low-energy electronic structure. In particular, we find that the dominant orbital for the pairing may change between z^2 and $x^2 - y^2$ when the position of the bonding z^2 band is varied by tuning either the c -axis lattice constant or electron concentration strength. We discuss the implications of these results for the superconductivity in both bulk $\text{La}_3\text{Ni}_2\text{O}_7$ and its thin film counterpart.

Introduction. The recent discovery of high-temperature superconductivity in bilayer nickelate $\text{La}_3\text{Ni}_2\text{O}_7$ with a transition temperature (T_c) of about 80 K under high pressure has sparked significant research interest [1]. Subsequent measurements on this compound and related $\text{La}_2\text{PrNi}_2\text{O}_7$ point to the bulk nature of the superconducting state [2, 3] despite possible structural imperfections [4–6]. In contrast to the infinite-layer nickelate $(\text{Sr}, \text{Nd})\text{NiO}_2$ thin films [7], for which the Ni^{2+} ion has the same $3d^9$ electron configuration as the high- T_c cuprates [8], $\text{La}_3\text{Ni}_2\text{O}_7$ has a unique $\text{Ni}^{2.5+}$ valence state with a $3d^{7.5}$ electron configuration. This configuration implicates multiplicity of the active $3d$ orbitals, as is the case for the Fe-based superconductors [9–11]. Together with the restriction to the z^2 and $x^2 - y^2$ $3d$ orbitals in the low energy sector [12], it leads to a bilayer two-orbital Hubbard model with the active electron count of $N = 3$ per unit cell. This encourages the expectation that orbital-selective electron correlation effects are important to the electronic structure of the system [13–21]. These considerations are also anchored on experimental results at ambient pressure: A recent optical conductivity measurement [22] revealed a substantially reduced Drude weight, and an angle-resolved photoemission spectroscopy (ARPES) measurement [23] found strongly orbital-dependent enhancement of the effective mass in the band structure. Taken together, these considerations suggest that $\text{La}_3\text{Ni}_2\text{O}_7$ is in proximity to an orbital-selective Mott phase with its multiband electronic structure strongly renormalized by the interactions. A global phase diagram [Fig. 1(a)] for the orbital-selective correlations has recently been advanced [21], anchored by the half-filling case $N = 4$. The purpose of the present

work is to explore the consequence of such correlations for superconductivity and explore the richness in the pairing states that could arise.

An added motivation comes from the very recent and rapidly growing experimental reports on superconductivity in thin films of bilayer nickelates at ambient pressure [24–28]. In these systems, superconductivity has been observed for films grown on the LaSrAlO_4 substrate with a compressed average in-plane lattice constant compared to the bulk counterpart under ambient pressure, and the observed T_c varies from 2 K to 30 K, which is in general lower than that in the bulk materials. Thin films also exhibit distinct structural property and electronic structure from the bulk. First, though the in-plane lattice constant is compressed in the film, the out-of-plane (c -axis) lattice constant is expanded due to the strain effect [24–27]. This modifies the interlayer coupling between the two Ni ions. Second, a recent ARPES measurement [29] on the superconducting $\text{La}_2\text{PrNi}_2\text{O}_7$ thin film found a sizable hole pocket, likely associated with the z^2 bonding band, and the entire system is about 0.2 hole per Ni doped from the Ni $3d^{7.5}$ configuration. A hole doping scenario is definitely different from the bulk case, which is via pressure tuning. These observations raise a number of questions: What are the key ingredients for superconductivity in thin films? Does the thin films' superconductivity arise in the same way as it does in the bulk materials? Notwithstanding the extensive theoretical interest in the superconductivity of the bilayer nickelates [13, 30–66], the issues as outlined above regarding superconductivity have yet to be analyzed theoretically.

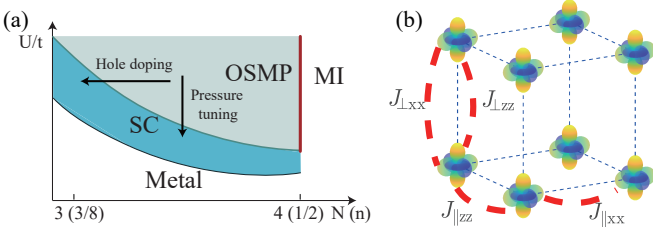


FIG. 1. (a) Global phase diagram of orbital-selective correlations, in the parameter space of U/t and electron occupation number at nonzero Hund's coupling J_H of the bilayer two-orbital Hubbard model for $\text{La}_3\text{Ni}_2\text{O}_7$ [21]. The red line denotes a Mott insulator (MI) where both orbitals are localized. The light shaded regime away from half-filling stands for an orbital-selective Mott phase (OSMP) where electrons in the z^2 orbital are localized while those in the $x^2 - y^2$ orbital remain itinerant. The system exhibits strong orbital-selective behavior near the OSMP and becomes superconducting (SC) at low temperatures. Conceptually, starting from within the OSMP, SC can develop by either pressure or hole doing. (b) Illustration of the orbital-dependent intralayer and interlayer exchange couplings in the bilayer two-orbital t - J model.

In this Letter, we do so by studying the superconducting pairing of the bilayer nickelates with the particular attention on the orbital-selective electronic correlations. Anchored by the global phase diagram in Fig. 1(a), which characterizes the strong orbital-selective behavior through a proximity to a two-orbital Mott insulator [21], superconductivity can be understood as arising by either pressure tuning (which reduces the correlation strength) or carrier doping. The proximate Mott nature provides the basis for the emergence of an effective bilayer two-orbital t - J model, which we use to study the superconductivity. We show that the dominant superconducting pairing state has either an extensive s -wave or a $d_{x^2-y^2}$ -wave symmetry with the gap anisotropy influenced by the interlayer exchange couplings. Moreover, we find that tuning the position of the z^2 bonding band by either strain effect or hole doping can induce an orbital-selective pairing crossing, with the dominant orbital contribution to the pairing channel changing from z^2 to $x^2 - y^2$. These results shed light on the nature of the superconducting states in both bulk bilayer nickelates and related thin films.

Model and method. To consider the electron correlation effects in $\text{La}_3\text{Ni}_2\text{O}_7$, we start from a bilayer two-orbital Hubbard model [21]. The slave-spin calculation on this model suggests that the system with $N = 3$ electrons per unit cell is in proximity to a putative Mott insulator at $N = 4$ and exhibits strong orbital-selective Mott behavior, as illustrated in Fig. 1(a). The low-energy effective model capturing the strong correlation effects is then a bilayer two-orbital t - J

model [13], with the Hamiltonian that reads

$$\mathcal{H} = \sum_{i\delta\alpha\beta\sigma} \frac{\sqrt{Z_\alpha Z_\beta}}{2} t_\delta^{\alpha\beta} f_{i\alpha\sigma}^\dagger f_{i+\delta\beta\sigma} + \sum_{i\alpha\sigma} (\epsilon'_\alpha - \mu) f_{i\alpha\sigma}^\dagger f_{i\alpha\sigma} + \sum_{i\delta\alpha} J_{\delta\alpha\alpha} (\mathbf{S}_{i\alpha} \cdot \mathbf{S}_{i+\delta\alpha} - \frac{1}{4} n_{i\alpha} n_{i+\delta\alpha}) \quad (1)$$

Here we have employed the slave-spin method [67–69] to renormalize the kinetic part of the Hamiltonian, with Z_α the quasiparticle spectral weight of the α orbital. We take the Z_α values of corresponding U and Hund's coupling J_H from the calculation in Ref. [21]. $f_{i\alpha\sigma}^\dagger$ creates a spinon at site i , in orbital α , and spin projection σ . ϵ'_α refers to the renormalized energy level of orbital α , μ is the chemical potential, and $t_\delta^{\alpha\beta}$ the hopping matrix along the δ ($= \hat{x}, \hat{y}, \hat{z}$) direction of the tight-binding model. The orbital index $\alpha = z, x$ correspond to the z^2 and $x^2 - y^2$ orbitals, respectively. The spin operator of the local moment is defined as $\mathbf{S}_{i\alpha} = \frac{1}{2} \sum_{ss'} f_{i\alpha s}^\dagger \boldsymbol{\sigma}_{ss'} f_{i\alpha s'}$, where $\boldsymbol{\sigma}$ represents the Pauli matrices. This approach is a generalization of the slave-boson theory [8, 13, 70] to the finite U and multiorbital case.

The effects of electron correlations have been taken into account by the renormalized electronic structure and the orbital-dependent intralayer and interlayer exchange interactions $J_{\parallel\alpha\alpha}$ and $J_{\perp\alpha\alpha}$. Here we keep only the leading exchange interactions as illustrated in Fig. 1(b). We assume the intralayer exchange couplings take the strong-coupling form $J_{\parallel\alpha\alpha} = 4t_{\parallel\alpha\alpha}^2/U$. It is expected that the interlayer exchange couplings are sizable. To examine their effects, we treat them over a parameter range in the model. Note that here we also include an effective interlayer coupling in the $x^2 - y^2$ orbital, $J_{\perp xx}$, which can be mediated through the strong Hund's coupling [61].

The superconducting pairing in the model of Eq.(1) is studied by a Bogoliubov Hubbard-Stratonovich decomposition of the exchange interactions in the spin singlet sector:

$$J_{\delta\alpha\alpha} \left(\mathbf{S}_{i\alpha} \cdot \mathbf{S}_{i+\delta\alpha} - \frac{1}{4} n_{i\alpha} n_{i+\delta\alpha} \right) \approx -\frac{1}{2} \left(\hat{\Delta}_{\delta\alpha}^\dagger \hat{\Delta}_{\delta\alpha} + \text{h.c.} - |\Delta_{\delta\alpha}|^2 \right), \quad (2)$$

where $\hat{\Delta}_{\delta\alpha} = f_{i\alpha\downarrow} f_{i+\delta\alpha\uparrow} - f_{i\alpha\uparrow} f_{i+\delta\alpha\downarrow}$, and the gap function $\Delta_{\delta\alpha} = \langle \hat{\Delta}_{\delta\alpha} \rangle$ is solved in a self-consistent way [71]. The superpositions of these gap functions then transform according to different irreducible representations of the D_{4h} group, with either s - or d -wave symmetry [13]. A complete symmetry classification is presented in the Supplemental Materials (SM) [72].

Superconducting pairing symmetry. We study how the superconducting pairing amplitude evolves with the interlayer exchange couplings $J_{\perp xx}$ and $J_{\perp zz}$, and a typical phase diagram for $U = 4.8$ eV and $J_H/U = 0.2$ is

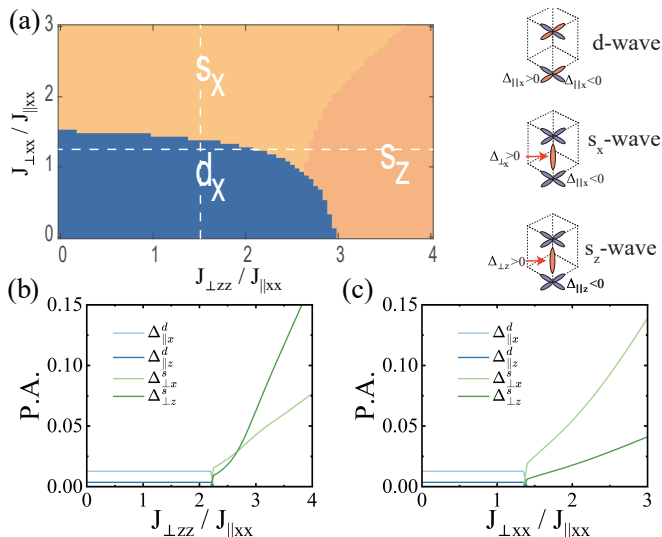


FIG. 2. (a) Superconducting phase diagram with $J_{\perp xx}$ and $J_{\perp zz}$ at $U = 4.8$ eV, which gives $J_{\parallel xx}/W = 0.05$ and $J_{\perp zz}/W = 0.0125$, where W is the bandwidth of the tight-binding part of the bilayer two-orbital model. Here d_x , s_x , and s_z refer to distinct leading pairing symmetries. d_x denotes the $d_{x^2-y^2}$ -wave B_{1g} symmetry with in-plane pairing in the $x^2 - y^2$ orbital, while $s_{x(z)}$ represents the extensive s -wave A_{1g} symmetry with interlayer pairing in the $x^2 - y^2$ (z^2) orbital. Real-space pairing structures of these three channels are illustrated in the right column of panel (a). (b) Evolution of dominant pairing amplitudes (P.A.) along the horizontal dashed line $J_{\perp xx}/J_{\parallel xx} = 1.2$ in panel (a), showing transition and crossover of the pairing symmetry with the interlayer exchange coupling $J_{\perp zz}$. (c) Same as (b) but along $J_{\perp zz}/J_{\parallel xx} = 1.5$.

shown in Fig. 2(a). For other U and J_H values generating the strong correlation effects, the phase diagram looks similarly. In this phase diagram the leading pairing channel has either a $d_{x^2-y^2}$ -wave B_{1g} or an extensive s -wave A_{1g} symmetry. The d -wave channel is dominant by the in-plane pairing of electrons in the $x^2 - y^2$ orbital, which is stabilized in the weak interlayer coupling regime of the phase diagram. Pairing amplitudes of several leading pairing channels are shown in Fig. 2(b) and (c), and those in all channels are shown in Fig. S1 of the SM [72]. From these results we see that increasing either $J_{\perp zz}$ or $J_{\perp xx}$, the pairing symmetry transitions to s -wave where the dominant gap function is the interlayer pairing. It can be either $\Delta_{\perp z}^s$ within the z^2 orbital or $\Delta_{\perp x}^s$ within the $x^2 - y^2$ orbital, depending on the strength of $J_{\perp xx}$ and $J_{\perp zz}$. These two regimes, both with the s -wave symmetry, are separated by a crossover as shown in the phase diagram of Fig. 2(a). In a broad regime of the s -wave pairing phase we find the in-plane gap function has opposite sign to the interlayer one in the leading pairing orbital, as illustrated in the right column of Fig. 2(a). Such a sign structure helps stabilize the superconductivity by avoiding nodes on the Fermi

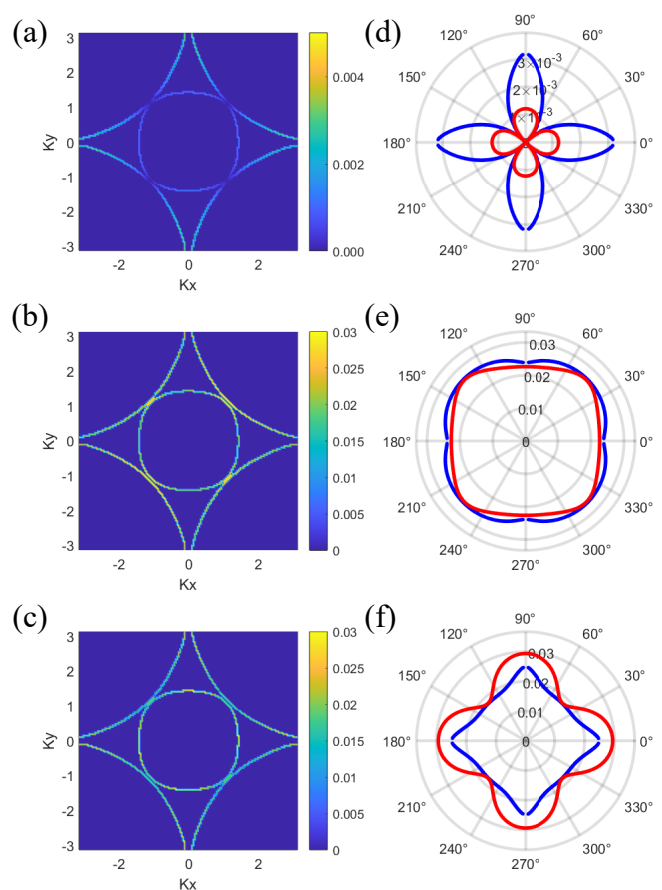


FIG. 3. Superconducting gaps projected onto the Fermi surface in phases with different pairing symmetries and corresponding angular dependence of the gaps: (a) and (d) for d -wave pairing at $J_{\perp xx}/J_{\parallel xx} = 0.5$ and $J_{\perp zz}/J_{\parallel xx} = 2.5$; (b) and (e) for s_x -wave pairing at $J_{\perp xx}/J_{\parallel xx} = 2.5$ and $J_{\perp zz}/J_{\parallel xx} = 2.5$; (c) and (f) for s_z -wave pairing at $J_{\perp xx}/J_{\parallel xx} = 1$ and $J_{\perp zz}/J_{\parallel xx} = 4$.

surface (see below). The evolution of pairing symmetry highlights the sensitivity of the superconducting state to the relative strengths of interlayer exchange interactions. Notably, along the boundaries between the s -wave and d -wave phases, a mixed $s + id$ pairing symmetry may emerge [71, 73]. However, this state is found to be nearly degenerate in energy with the pure d -wave phase and thus is not explicitly marked in the phase diagram.

We next investigate the distribution of the superconducting gap on the Fermi surface. Representative results at specific parameter sets corresponding to the d_x , s_x , and s_z pairing are shown in Fig. 3. For the d -wave pairing, the gap function, taking the form of $\Delta_{\parallel}^d(k) \propto \cos(k_x) - \cos(k_y)$, changes sign across $k_x = \pm k_y$ and features nodes along these two directions. This causes strongly anisotropic superconducting gap. In contrast, the s -wave phase is fully gapped and nodeless because the dominant interlayer pairing Δ_{\perp}^s enforces a uniform gap structure without any sign

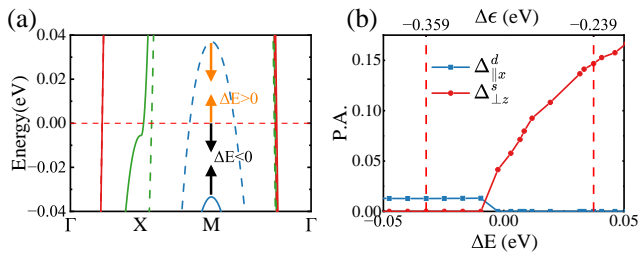


FIG. 4. (a) Band structures with different crystal splitting $\Delta\epsilon = -0.239$ eV (dashed line) and $\Delta\epsilon = -0.359$ eV (solid line), respectively. ΔE denotes the energy of the z^2 bonding band top to the Fermi level, which is sensitive to $\Delta\epsilon$. (b) Leading pairing amplitudes (P.A.) as a function of ΔE and $\Delta\epsilon$ showing a transition between d -wave and s -wave pairing symmetry. The exchange couplings are taken to be $J_{\perp zz}/J_{\parallel xx} = 2.0$ and $J_{\perp xx}/J_{\parallel xx} = 0.5$.

change. However, strong competition between pairing in the two orbitals as well as the interplay between the interlayer pairing Δ_{\perp}^s and the intralayer pairing $\Delta_{\parallel}^s \propto \cos(k_x) + \cos(k_y)$ cause a complex gap structure that cannot be described by a single gap function and may give rise to anisotropic superconducting gap. These are reflected in the primarily distinct gap anisotropies in the s_x and s_z regimes of the phase diagram. In the s_x regime, the gap is almost isotropic with minima along the $\pm k_x/k_y$ direction. But in the s_z regime, due to the influence of the subleading pairing in the $x^2 - y^2$ orbital, the gaps on the Fermi surfaces can exhibit substantial anisotropy with gap minima along the $k_x = \pm k_y$ direction.

Pairing crossing between the z^2 and $x^2 - y^2$ orbitals induced by the shift of the z^2 bonding band. We now investigate the evolution of superconducting pairing symmetry as a function of the top position of the z^2 orbital bonding band (near the M point of the Brillouin zone); ΔE marks the separation of this band top to the Fermi level. We tune ΔE by varying the crystal splitting between the $x^2 - y^2$ and z^2 orbitals, $\Delta\epsilon = \epsilon'_z - \epsilon'_x$, in the tight-binding part of the Hamiltonian. As shown in Fig. 4 for $J_{\perp zz}/J_{\parallel xx} = 2.0$ and $J_{\perp xx}/J_{\parallel xx} = 0.5$, when $\Delta E > 0$, where the z^2 bonding band crosses the Fermi level, we find the leading pairing symmetry is always s_z . Decreasing ΔE to negative value, where the z^2 bonding band sinks to below the Fermi level, the leading pairing symmetry transitions to d_x . Comparing to the s_z pairing, the pairing amplitude of the d_x channel is largely reduced and becomes almost independent of ΔE away from the transition regime. In other regimes of the phase diagram, a similar crossover between the s_z and s_x pairing induced by ΔE can take place, as shown in Fig. S2 of the SM [72]. Such a crossover/transition between the z^2 and $x^2 - y^2$ orbital pairing can be understood as follows: The system contains singlet pairing of electrons in the z^2 orbital between the top and bottom layers. Once the

z^2 orbital bonding band crosses the Fermi level, the coherent movement of these prepared electrons become superconducting with the s -wave symmetry. On the other hand, when the z^2 orbital bonding band is below the Fermi level, though the electrons could be locally paired, a global coherence is not established within the z^2 orbital, given its proximity to the Mott localization. In this limit, however, the superconductivity can be carried by electrons in the $x^2 - y^2$ orbital, with a d -wave (or an s -wave) symmetry. Given the in-plane pairing structure and the much weaker interlayer hopping in the $x^2 - y^2$ orbital, the pairing amplitude of the d_x pairing is almost independent of ΔE and largely reduced compared to the s_z -wave case.

Discussion and conclusion. In our calculations, the strong orbital-selective correlations affect the superconducting pairing via both renormalizing the non-interacting electronic structure and inducing orbital-dependent exchange interactions. As a result, the leading pairing channel is generally orbital dependent, dominated by either z^2 or $x^2 - y^2$ orbital, as shown in the phase diagram of Fig. 2(a). In particular, delocalization of electrons in the z^2 orbital from the OSMP (Fig. 1(a)) plays a crucial role in stabilizing the s -wave pairing. This orbital may directly participate in superconductivity, causing the s_z pairing in the phase diagram. In this regime the itinerancy of electrons in this orbital helps establish a global phase coherence of the superconductivity. Even in the s_x regime where the dominant pairing originates from the $x^2 - y^2$ orbital, the z^2 orbital helps mediate pairing by enhancing $J_{\perp xx}$ through Hund's coupling.

Our results also show that the ratio of interlayer to intralayer exchange coupling is important for determining the superconducting state in $\text{La}_3\text{Ni}_2\text{O}_7$. Based on a previous slave-spin calculation [21] we roughly estimate $J_{\perp zz}/J_{\parallel xx} \sim 1-3$ and $J_{\perp xx} < J_{\perp zz}$. Correspondingly, the system is in a regime of the phase diagram where d_x , s_x , and s_z pairing channels are in strong competition. Note that although our estimated exchange couplings are within the same order as those suggested by resonant inelastic X-ray scattering and inelastic neutron scattering measurements at ambient pressure [74, 75], precise determination of the values awaits future experimental and theoretical studies. Examining the gap anisotropy would be very helpful to determine the pairing symmetry. However, as shown in Fig. 3, both the d_x and s_z pairing can be strongly anisotropic and the gap minima of the two are located along the same direction of the Brillouin zone. Therefore, phase sensitive measurements would be necessary to distinguish these two pairing symmetries.

As shown in Fig. 4, the pairing symmetry can be sensitive to the position of the z^2 bonding band, which can be tuned by either carrier doping or crystal field splitting $\Delta\epsilon$. Note that the evolution of superconductivity we find here crucially depends on the

change in the Fermi surface and, thus, is different from what happens to the effect of crystal field splitting in certain weak-coupling context [76]. In our theory, increasing $\Delta\epsilon$ raises the onsite energy of the z^2 orbital, corresponding to hole doping the z^2 bonding band while electron doping the $x^2 - y^2$ orbital. In real materials, $\Delta\epsilon$ is closely related to the out-of-plane lattice constant c . Increasing c elongates the outer Ni-O bond distances and reduces the onsite energy of the z^2 orbital, ϵ_z . As already mentioned, this may trigger a transition of the pairing symmetry from s_z to d_x by pushing the z^2 bonding band to be below the Fermi level. Note that the pairing amplitude of the d -wave channel is largely reduced. This may explain why T_c is significantly reduced in $\text{La}_3\text{Ni}_2\text{O}_7$ thin films [24]: In the films, c is elongated compared to the bulk counterpart as a strain effect by compressing the in-plane lattice constants; according to our results, the pairing in these thin films could be d -wave, in contrast to the likely s -wave in the bulk. Following this idea, we examine the pressure effects in the bulk. The hydrostatic pressure would compress both in-plane and out-of-plane lattice constants. With c compressed, the z^2 bonding band is raised across the Fermi level, which is likely to stabilize the s -wave pairing with a high T_c . As for the recently observed superconductivity in $\text{La}_2\text{PrNi}_2\text{O}_7$ thin films [25, 27], an ARPES study implicates an effective hole doping as playing a crucial role in stabilizing the T_c up to about 30 K. It is possible that in this material, there is strong competition between effects of the crystal field splitting and hole doping, such that the pairing symmetry stays the same as in the bulk system under pressure.

In conclusion, based on the strong orbital-selective correlations and proximity to a Mott insulator, we consider an effective bilayer two-orbital t - J model to study the superconducting pairing of $\text{La}_3\text{Ni}_2\text{O}_7$. We present a phase diagram with respect to the interlayer exchange couplings and find the leading pairing to have either an extensive s -wave or a $d_{x^2-y^2}$ -wave symmetry. We show that tuning the position of the z^2 bonding band by either strain effect or carrier doping can induce a transition between z^2 and $x^2 - y^2$ orbital contribution to the leading pairing channel. These results help elucidate the puzzling superconducting states in both the bulk bilayer nickelates and their thin film counterparts.

We thank W. Ding, H. Y. Hwang, W. Ku, W. Li, K.-S. Lin, X. Lu, L. Sun, F. Wang, M. Wang, C. Wu, F. Yang, Y.-f. Yang, and G.-M. Zhang for useful discussions. This work has in part been supported by the National Science Foundation of China (Grants 12334008 and 12174441). Work at Rice was primarily supported by the U.S. Department of Energy, Office of Science, Basic Energy Sciences, under Award No. DE-SC0018197, and by the Robert A. Welch Foundation Grant No. C-1411. Q.S. acknowledges the hospitality of the Aspen Center for Physics, which is supported by the NSF grant No. PHY-2210452.

* rong.yu@ruc.edu.cn

† qmsi@rice.edu

- [1] H. Sun, M. Huo, X. Hu, J. Li, Z. Liu, Y. Han, L. Tang, Z. Mao, P. Yang, B. Wang, et al., *Nature* **621**, 493 (2023).
- [2] Y. Zhang, D. Su, Y. Huang, Z. Shan, H. Sun, M. Huo, K. Ye, J. Zhang, Z. Yang, Y. Xu, et al., *Nat. Phys* **20**, 1269–1273 (2024), ISSN 1745-2481, URL <http://dx.doi.org/10.1038/s41567-024-02515-y>.
- [3] N. Wang, G. Wang, X. Shen, J. Hou, J. Luo, X. Ma, H. Yang, L. Shi, J. Dou, J. Feng, et al., arXiv preprint arXiv:2407.05681 (2024).
- [4] Z. Dong, M. Huo, J. Li, J. Li, P. Li, H. Sun, L. Gu, Y. Lu, M. Wang, Y. Wang, et al., *Nature* **630**, 847–852 (2024), ISSN 1476-4687.
- [5] H. Wang, L. Chen, A. Rutherford, H. Zhou, and W. Xie, *Inorg. Chem.* **63**, 5020 (2024).
- [6] Y. Zhou, J. Guo, S. Cai, H. Sun, C. Li, J. Zhao, P. Wang, J. Han, X. Chen, Y. Chen, et al., *Mater. Radiat. Extremes* **10** (2025).
- [7] D. Li, K. Lee, B. Y. Wang, M. Osada, S. Crossley, H. R. Lee, Y. Cui, Y. Hikita, and H. Y. Hwang, *Nature* **572**, 624 (2019).
- [8] P. A. Lee, N. Nagaosa, and X.-G. Wen, *Rev. Mod. Phys.* **78**, 17 (2006).
- [9] Q. Si, R. Yu, and E. Abrahams, *Nat. Rev. Mater.* **1**, 16017 (2016).
- [10] A. E. Böhrmer, J.-H. Chu, S. Lederer, and M. Yi, *Nat. Phys* **18**, 1412 (2022).
- [11] Q. Si and N. E. Hussey, *Phys. Today* **76**, 34 (2023).
- [12] Z. Luo, X. Hu, M. Wang, W. Wú, and D.-X. Yao, *Phys. Rev. Lett* **131**, 126001 (2023).
- [13] Z. Liao, L. Chen, G. Duan, Y. Wang, C. Liu, R. Yu, and Q. Si, *Phys. Rev. B* **108**, 214522 (2023).
- [14] D. Shilenko and I. Leonov, *Phys. Rev. B* **108**, 125105 (2023).
- [15] F. Lechermann, J. Gondolf, S. Bötzel, and I. M. Eremin, *Phys. Rev. B* **108**, L201121 (2023).
- [16] Y. Zhang, L.-F. Lin, A. Moreo, and E. Dagotto, *Phys. Rev. B* **108**, L180510 (2023).
- [17] Y. Cao and Y.-f. Yang, *Phys. Rev. B* **109**, L081105 (2024).
- [18] Z. Ouyang, J.-M. Wang, J.-X. Wang, R.-Q. He, L. Huang, and Z.-Y. Lu, *Phys. Rev. B* **109**, 115114 (2024).
- [19] S. Rye, N. Witt, and T. O. Wehling, *Phys. Rev. Lett* **133**, 096002 (2024).
- [20] Y.-H. Tian, Y. Chen, J.-M. Wang, R.-Q. He, and Z.-Y. Lu, *Phys. Rev. B* **109**, 165154 (2024).
- [21] Z. Liao, Y. Wang, L. Chen, G. Duan, R. Yu, and Q. Si, arXiv preprint arXiv:2412.21019 (2024).
- [22] Z. Liu, M. Huo, J. Li, Q. Li, Y. Liu, Y. Dai, X. Zhou, J. Hao, Y. Lu, M. Wang, et al., *Nat. Commun* **15**, 7570 (2024).
- [23] J. Yang, H. Sun, X. Hu, Y. Xie, T. Miao, H. Luo, H. Chen, B. Liang, W. Zhu, G. Qu, et al., *Nat. Commun* **15**, 4373 (2024).
- [24] E. K. Ko, Y. Yu, Y. Liu, L. Bhatt, J. Li, V. Thampy, C.-T. Kuo, B. Y. Wang, Y. Lee, K. Lee, et al., *Nature* (2024), ISSN 1476-4687, URL <http://dx.doi.org/10.1038/s41586-024-08525-3>.
- [25] G. Zhou, W. Lv, H. Wang, Z. Nie, Y. Chen, Y. Li, H. Huang, W. Chen, Y. Sun, Q.-K. Xue, et al., arXiv

- preprint arXiv:2412.16622 (2024).
- [26] L. Bhatt, A. Y. Jiang, E. K. Ko, N. Schnitzer, G. A. Pan, D. F. Segedin, Y. Liu, Y. Yu, Y.-F. Zhao, E. A. Morales, et al., arXiv preprint arXiv:2501.08204 (2025).
- [27] Y. Liu, E. K. Ko, Y. Tarn, L. Bhatt, B. H. Goodge, D. A. Muller, S. Raghu, Y. Yu, and H. Y. Hwang, arXiv preprint arXiv:2501.08022 (2025).
- [28] C. Yue, J.-J. Miao, H. Huang, Y. Hua, P. Li, Y. Li, G. Zhou, W. Lv, Q. Yang, H. Sun, et al., arXiv preprint arXiv:2501.06875 (2025).
- [29] P. Li, G. Zhou, W. Lv, Y. Li, C. Yue, H. Huang, L. Xu, J. Shen, Y. Miao, W. Song, et al., arXiv preprint arXiv:2501.09255 (2025).
- [30] X.-Z. Qu, D.-W. Qu, W. Li, and G. Su, arXiv preprint arXiv:2311.12769 (2023).
- [31] Y. Wang, K. Jiang, Z. Wang, F.-C. Zhang, and J. Hu, Phys. Rev. B **110**, 205122 (2024).
- [32] G. Heier, K. Park, and S. Y. Savrasov, Phys. Rev. B **109**, 104508 (2024).
- [33] J. Zhan, Y. Gu, X. Wu, and J. Hu, arXiv preprint arXiv:2404.03638 (2024).
- [34] W.-X. Chang, S. Guo, Y.-Z. You, and Z.-X. Li, arXiv preprint arXiv:2311.09970 (2023).
- [35] K. Jiang, Z. Wang, and F.-C. Zhang, Chin. Phys. Lett. **41**, 017402 (2024).
- [36] J. Huang, Z. Wang, and T. Zhou, Phys. Rev. B **108**, 174501 (2023).
- [37] J.-R. Xue and F. Wang, Chin. Phys. Lett. **41**, 057403 (2024).
- [38] J. Chen, F. Yang, and W. Li, Phys. Rev. B **110**, L041111 (2024).
- [39] T. Kaneko, H. Sakakibara, M. Ochi, and K. Kuroki, Phys. Rev. B **109**, 045154 (2024).
- [40] H. Sakakibara, N. Kitamine, M. Ochi, and K. Kuroki, Phys. Rev. Lett. **132**, 106002 (2024).
- [41] R. Jiang, J. Hou, Z. Fan, Z.-J. Lang, and W. Ku, Phys. Rev. Lett. **132**, 126503 (2024).
- [42] H. Liu, C. Xia, S. Zhou, and H. Chen, arXiv preprint arXiv:2311.07316 (2023).
- [43] H. Yang, H. Oh, and Y.-H. Zhang, arXiv preprint arXiv:2408.01493 (2024).
- [44] H. Yang, H. Oh, and Y.-H. Zhang, Phys. Rev. B **110**, 104517 (2024).
- [45] J.-X. Zhang, H.-K. Zhang, Y.-Z. You, and Z.-Y. Weng, Phys. Rev. Lett. **133**, 126501 (2024).
- [46] D.-C. Lu, M. Li, Z.-Y. Zeng, W. Hou, J. Wang, F. Yang, and Y.-Z. You, arXiv preprint arXiv:2308.11195 (2023).
- [47] Z. Fan, J.-F. Zhang, B. Zhan, D. Lv, X.-Y. Jiang, B. Normand, and T. Xiang, Phys. Rev. B **110**, 024514 (2024).
- [48] Y.-Y. Zheng and W. Wú, Phys. Rev. B **111**, 035108 (2025).
- [49] H. Schlömer, U. Schollwöck, F. Grusdt, and A. Bohrdt, Commun. Phys. **7**, 366 (2024).
- [50] S. Bötzel, F. Lechermann, J. Gondolf, and I. M. Eremin, Phys. Rev. B **109**, L180502 (2024).
- [51] H. Oh, B. Zhou, and Y.-H. Zhang, arXiv preprint arXiv:2405.00092 (2024).
- [52] C. Le, J. Zhan, X. Wu, and J. Hu, arXiv preprint arXiv:2501.14665 (2025).
- [53] Y.-B. Liu, H. Sun, M. Zhang, Q. Liu, W.-Q. Chen, and F. Yang, arXiv preprint arXiv:2501.14752 (2024).
- [54] Z.-Y. Shao, Y.-B. Liu, M. Liu, and F. Yang, arXiv preprint arXiv:2501.10409 (2025).
- [55] X.-Z. Qu, D.-W. Qu, J. Chen, C. Wu, F. Yang, W. Li, and G. Su, Phys. Rev. Lett. **132**, 036502 (2024).
- [56] Z. Pan, C. Lu, F. Yang, and C. Wu, Chin. Phys. Lett. **41**, 087401 (2024).
- [57] J. Wang and Y.-f. Yang, arXiv:2408.09774 (2024).
- [58] Q. Qin and Y.-f. Yang, Phys. Rev. B **108**, L140504 (2023).
- [59] Z. Luo, B. Lv, M. Wang, W. Wú, and D.-X. Yao, npj Quantum Mater. **9**, 61 (2024).
- [60] Y.-f. Yang, G.-M. Zhang, and F.-C. Zhang, Phys. Rev. B **108**, L201108 (2023).
- [61] C. Lu, Z. Pan, F. Yang, and C. Wu, Phys. Rev. Lett. **132**, 146002 (2024).
- [62] C. Lu, Z. Pan, F. Yang, and C. Wu, Phys. Rev. B **110**, 094509 (2024).
- [63] M. Kakoi, T. Kaneko, H. Sakakibara, M. Ochi, and K. Kuroki, Phys. Rev. B **109**, L201124 (2024).
- [64] R. Yu, T. Ma, and C. Wu, arXiv preprint arXiv:2408.02031 (2024).
- [65] Q.-G. Yang, D. Wang, and Q.-H. Wang, Phys. Rev. B **108**, L140505 (2023).
- [66] Y. Zhang, L.-F. Lin, A. Moreo, T. A. Maier, and E. Dagotto, Nat. Commun. **15**, 2470 (2024).
- [67] R. Yu and S. Qimiao, Phys. Rev. B **86**, 085104 (2012).
- [68] R. Yu and Q. Si, Phys. Rev. B **96**, 125110 (2017).
- [69] N. Lanata, H. U. Strand, X. Dai, and B. Hellsing, Phys. Rev. B **85**, 035133 (2012).
- [70] G. Kotliar, Phys. Rev. B **37**, 3664 (1988).
- [71] R. Yu, P. Goswami, Q. Si, P. Nikolic, and J.-X. Zhu, Nat. Commun. **4**, 2783 (2013).
- [72] See Supplemental Information [<http://link...>] for details about the classification of the superconducting pairing symmetry of the two-orbital t - J model, which also includes Refs. [13]. (2025).
- [73] H. Hu, R. Yu, E. M. Nica, J.-X. Zhu, and Q. Si, Phys. Rev. B **98**, 220503 (2018).
- [74] T. Xie, M. Huo, X. Ni, F. Shen, X. Huang, H. Sun, H. C. Walker, D. Adroja, D. Yu, B. Shen, et al., Sci. Bull. **69**, 3221 (2024).
- [75] X. Chen, J. Choi, Z. Jiang, J. Mei, K. Jiang, J. Li, S. Agrestini, M. Garcia-Fernandez, H. Sun, X. Huang, et al., Nat. Commun. **15**, 9597 (2024).
- [76] C. Xia, H. Liu, S. Zhou, and H. Chen, Nat. Commun. **16**, 1054 (2025).

SUPPLEMENTAL MATERIAL – Orbital-selective correlation effects and superconducting pairing symmetry in a multiorbital t - J model for bilayer nickelates

Guijing Duan¹, Zhiguang Liao¹, Lei Chen^{2,3}, Yiming Wang², Rong Yu^{1,4}, Qimiao Si²

¹*School of Physics and Beijing Key Laboratory of Opto-electronic Functional Materials and Micro-nano Devices, Renmin University of China, Beijing 100872, China*

²*Department of Physics & Astronomy, Extreme Quantum Materials Alliance, Smalley Curl Institute, Rice University, Houston, Texas 77005, USA*

³*Department of Physics and Astronomy, Stony Brook University, Stony Brook, NY 11794, USA*

⁴*Key Laboratory of Quantum State Construction and Manipulation (Ministry of Education), Renmin University of China, Beijing, 100872, China*

SYMMETRY CLASSIFICATION OF SUPERCONDUCTING GAP FUNCTIONS

Here we present a symmetry classification of the superconducting gap functions of the bilayer two-orbital t - J model by analyzing their transformation properties under the tetragonal D_{4h} group. We consider only the orbital diagonal exchange couplings in the model, and the gap functions are also orbital diagonal in this work. The resulting symmetry assignments in each orbital are summarized in Table S1. Basically, the in-plane s -wave and d -wave pairing channels are formed by linear combinations of the gap functions in the real space, *i.e.*, $\Delta_{\parallel}^{s/d} = \Delta_{\hat{x}} \pm \Delta_{\hat{y}}$. These in-plane s and d pairing channels have $\cos k_x \pm \cos k_y$ form factors, respectively. These pairing channels in the two layers are then combined to two, transforming symmetrically and antisymmetrically under the inversion symmetry (distinguished by the Pauli matrices η_0 and η_3 , respectively), respectively. For the interlayer pairing, $\Delta_{\perp}^s = \Delta_z$ is uniformly s -wave, given that the dominant interlayer exchange coupling corresponds to the nearest neighbor term J_{\perp} .

$\Delta(\mathbf{r})$	$\Delta(\mathbf{k})$	Symmetry
$(\Delta_{\hat{x}} + \Delta_{\hat{y}})\eta_0$	$s_{x^2+y^2}\eta_0$	A^{1g}
$(\Delta_{\hat{x}} - \Delta_{\hat{y}})\eta_0$	$d_{x^2-y^2}\eta_0$	B^{1g}
$(\Delta_{\hat{x}} + \Delta_{\hat{y}})\eta_3$	$s_{x^2+y^2}\eta_3$	A^{2u}
$(\Delta_{\hat{x}} - \Delta_{\hat{y}})\eta_3$	$d_{x^2-y^2}\eta_3$	B^{2u}
$\Delta_{\hat{z}}$	s_z	A^{1g}

TABLE S1. Superconducting pairing symmetry of the effective multiorbital t - J model. $\Delta(\mathbf{r})$ and $\Delta(\mathbf{k})$ refer to the gap functions in real and momentum space, respectively. Their symmetry is characterized by the corresponding irreducible representation of the tetragonal D_{4h} group. η_0 and η_3 refer to the 2×2 unit matrix and z -component of the Pauli matrices, respectively. $\hat{x}(\hat{y}, \hat{z})$ refers to the unit vector along the $x(y, z)$ direction.

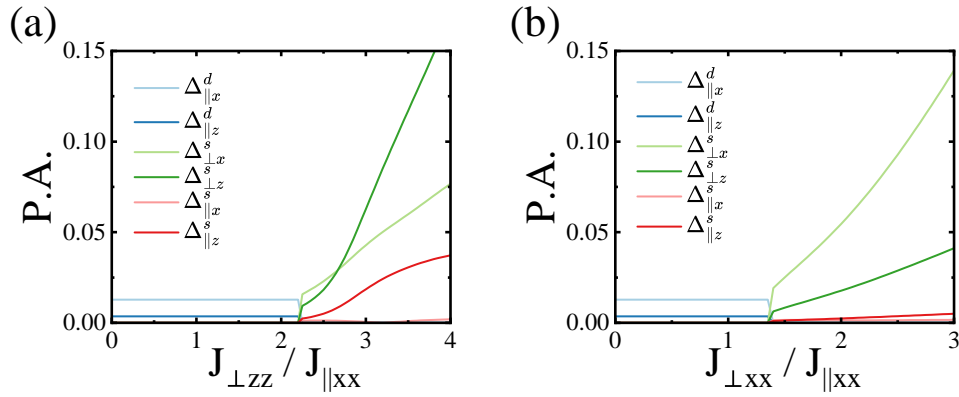


FIG. S1. (a) Evolution of all pairing amplitudes (P.A.) along the horizontal dashed line $J_{\perp xx}/J_{\parallel xx} = 1.2$ in Fig. 2(a). (b) Same as (a) but along $J_{\perp zz}/J_{\parallel xx} = 1.5$.

Pairing amplitudes along dashed lines corresponding to model parameters in Fig. 2 are shown in Fig. S1. In

the calculation, we find only three pairing channels in each orbital, $\Delta_{\perp x(z)}^s$, $\Delta_{\parallel x(z)}^s$ and $\Delta_{\parallel x(z)}^d$, with A^{1g} and B^{1g} symmetries, respectively. The pairing amplitudes of the leading pairing channels have been shown in Fig. 2(b) and (c). Here in Fig. S1 we present results of all non-zero pairing channels. The subleading channels evolve in the same way as the leading one with the same symmetry.

CROSS BETWEEN THE s_x AND s_z PAIRING INDUCED BY THE SHIFT OF THE z^2 BONDING BAND

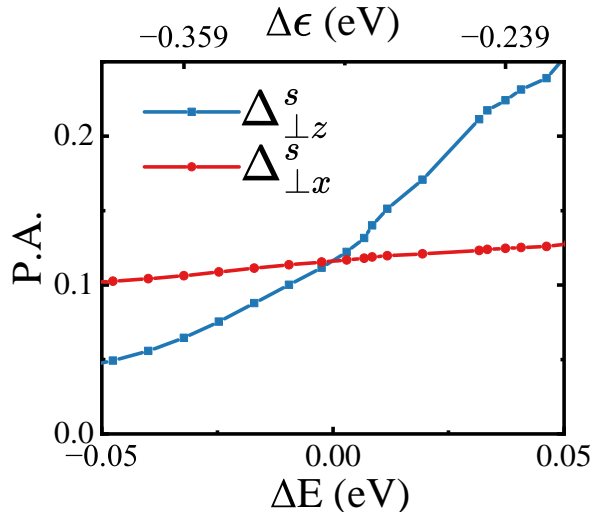


FIG. S2. Leading pairing amplitudes (P.A.) as a function of ΔE and $\Delta\epsilon$ that exhibit a crossover between the s_x and s_z pairing channels.

In addition to the transition between the s_z and d_x pairing symmetries induced by the shift of the z^2 bonding band as discussed in the main text, we observe similar pairing cross behavior in other regimes of the phase diagram. As shown in Fig. S2, for $J_{\perp zz}/J_{\parallel xx} = 2.5$ and $J_{\perp xx}/J_{\parallel xx} = 2.5$, the system exhibits a crossover between s_z and s_x pairing channels as the band top of the z^2 bonding band ΔE is varied. When the z^2 bonding band lies above the Fermi level ($\Delta E > 0$), the s_z pairing dominates, similar to the case discussed in the main text. As ΔE becomes negative and the z^2 bonding band sinks below the Fermi level, the leading pairing channel of the system crosses to be the s_x pairing. This demonstrates that the position of the z^2 bonding band relative to the Fermi level plays a crucial role in determining the exact pairing symmetry across different coupling regimes.